J. Appl. Comput. Mech., 5(1) (2019) 70-76
DOI: 10.22055/JACM.2018.25334.1247

ISSN: 2383-4536
jacm.scu.ac.ir

M&MoCS
Shahid Chamran University of Ahvaz

Journal of
Applied and Computational Mechanics

Research Paper

A Numerical Simulation of Inspiratory Airflow in Human Airways during Exercise at Sea Level and at High Altitude

Endalew Getnet Tsega [1], Vinod Kumar Katiyar [2]

[1] Department of Mathematics, Indian Institute of Technology Roorkee
Roorkee -247667 (Uttarakhand) India, endalebdumath2016@gmail.com,

[2] Department of Mathematics, Indian Institute of Technology Roorkee
Roorkee -247667 (Uttarakhand) India, vktmafma20@gmail.com

Received March 21 2018; Revised May 11 2018; Accepted for publication May 13 2018.
Corresponding author: Endalew Getnet Tsega, endalebdumath2016@gmail.com

Abstract. At high altitudes, the air pressure is much lower than it is at sea level and contains fewer oxygen molecules and less oxygen is taken in at each breath. This requires deeper and rapid breathing to get the same amount of oxygen into the blood stream compared to breathing in air at sea level. Exercises increase the oxygen demand and make breathing more difficult at high altitude. In this study, a numerical simulation of inspiratory airflow in a three-dimensional bifurcating human airways model (third to sixth generation) during exercise at sea level and at high altitude was performed. The computational fluid dynamics (CFD) solver FLUENT was used to solve the governing equations for unsteady airflow in the model. Flow velocity, pressure, and wall shear stress were obtained from the simulations with the two breathing conditions. The result of this study quantitatively showed that performing exercise with a given work rate at high altitude increased inspiratory airflow velocity, pressure, and wall shear stress more than that at sea level in the airway model. The ranges of the airflow fields were also higher at high altitude than sea level. The simulation results showed that there were no significant differences in flowing pattern for the two breathing conditions.

Keywords: Computational fluid dynamics; Airway model; Flow fields; Exercise; Sea level; High altitude; Numerical simulation.

1. Introduction

At high altitude, the density of the atmospheric gases is low and hence one take in less oxygen at each breath. As a result, the breathing rate is increased in an attempt to supply the body with sufficient oxygen. During exercise, the muscle cells respire more than they do at rest. This means oxygen and glucose must be delivered to them more quickly and waste carbon dioxide must be removed more quickly. This is achieved by increasing the breathing rate along with the heart rate. Therefore, the mechanics of breathing is highly affected during exercise at high altitude compared to that at sea level.

Cibella et al. [1] studied respiratory mechanics during exhaustive submaximal exercise at high altitude in healthy humans. Four healthy young human males (mean age, 34.2 years; range, 33-35 years) were observed in their study during exercise at sea level, the work rate of 225W and after a 28-day stay at 5050m high attitude, a barometric pressure of about 410mmHg and work rate of 173W. They found that during the last 10% fraction of exercise, the average air flow rate was 91.2 L/ min at sea level and 134 .3 L/ min at high altitude.

Aiken [2] believed that altitude training is a component of virtually all elite running programs- 95 percent of all medallists at the world championships and the Olympic Games since 1968 have either lived or trained at altitude. He added that professional athletes live at altitude or simulated altitude over the course of weeks or months and often come down to sea level to train, following the "Live High, Train Low" method shown to produce the greatest benefits. J. Wehrlin et al. [3] studied the altitude effect on running performance. They found that increases in altitude had a predictable linear effect on the oxygen consumption and the exercise performance. For every thousand feet of altitude increase above 1,000 feet above sea level, the oxygen consumption dropped by 1.9% and the time to exhaustion on a constant-speed treadmill run decreased by 4.4% per 1,000 feet of altitude.

Sheel et al. [4] noted that at higher levels of exercise intensity at high altitude, the work of breathing was 35-40% greater compared with the same exercise at sea level. Beyond a flow rate of 65 L/min at high altitude, the working of breathing was significantly increased relative to the sea-level exercise. It appears that the reduction air resistance at high altitude is offset by increasing turbulent flow produced by high flow rates.

Augusto et al. [5] noted that CFD is a tool which enables the simulation of velocity, pressure, and temperature fields as well as other transport phenomena. Numerical studies of airflow fluid dynamics and particle deposition inside the lungs first requires the construction of a morphological model representing the respiratory tract. The scheme that is most widely used to describe the human airways was created by Weibel [6]. Deng et al. [7] investigated particle deposition in human tracheobronchial airways for infants, children, and adults using CFD modelling. They developed 3-D symmetric triple bifurcation airway models (G3–G6 and G9–G12). The numerical calculation was done using the CFD software ANSYS Fluent Version 6.3. The governing equations were solved using the finite volume method (FVM). Srivastav et al. [8] used CFD technique to simulate airflow and aerosol-particle deposition in third to sixth generation human respiratory tract based on the Weibel model [6].

The aim of this study is to numerically investigate the effects of high altitude on the process of breathing during exercise. Numerical results of CFD simulations are used to compare and analyse the airflow dynamics for breathing during exercise at sea level and at high altitude. The study aims to provide quantitative information on exercising at high altitudes.

2. Methods

2.1 Airway Geometry

The symmetric bifurcation tracheobronchial airway model (G3-G6) using SOLIDWORKS, 3D CAD design software was constructed. The length and diameter of each generation was based on the Weibel model. The mathematical description of the morphologically realistic bifurcation model of Hegedűs et al. [9] was taken into consideration in the construction. The ratio of outer radius of curvature of a bifurcation (R) to the daughter diameter is set to 2 as done by Ou et al. [10] and the ratio of the carinal radius of curvature (r) to the daughter diameter was set 0.1 as done by Ou et al. [11] in the construction. The angle of branching was set to 350. The detail of geometric dimension is summarized in Table 1 and Fig. 1. L is the length of the airway and D is its diameter.

Table 1. The geometric dimension of the model

Generation	L(mm)	D(mm)	R(mm)	r(mm)
G3	7.6	5.6	9.0	0.45
G4	12.7	4.5	7.0	0.35
G5	10.7	3.5	5.6	0.28
G6	9.0	2.8	-	-

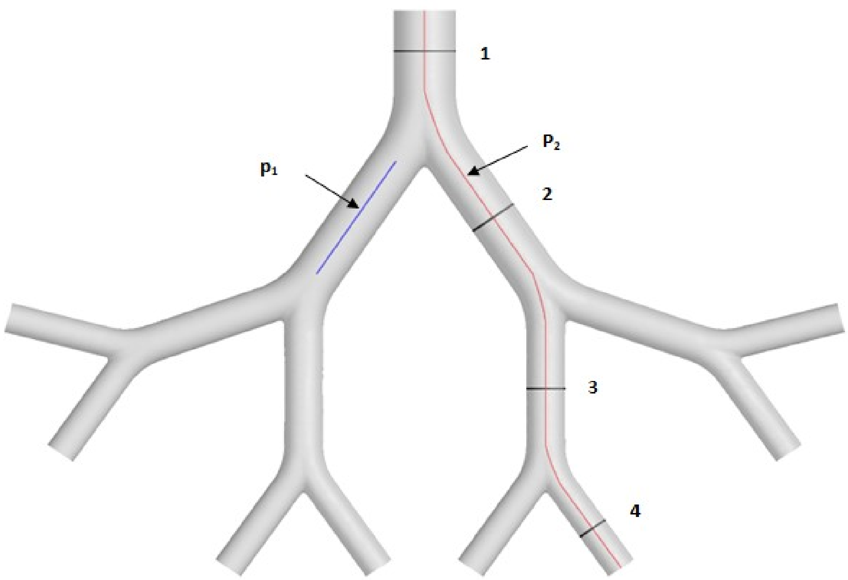

Fig. 1. Three-dimensional four generations (G3-G6) bifurcation airway model.

2.2 Governing Equations

The air is assumed to be an incompressible Newtonian fluid. The governing equations for unsteady-state airflow in respiratory tract are the continuity and Navier-Stokes equations for the viscous incompressible Newtonian fluid. In vector notation,

$$\nabla.\mathbf{v}=0 \tag{1}$$

$$\rho(\frac{\partial \mathbf{v}}{\partial t}+\mathbf{v}.\nabla \mathbf{v})=-\nabla p+\mu\nabla^{2}\mathbf{v} \tag{2}$$

where v is velocity vector, p is static pressure, ρ is density, and μ is dynamic viscosity of the air.

2.3 Boundary Conditions

Input flow rates investigated by Cibella et al. [1], 91.2 L/ min (for work rate of 225W) at sea level and 134 .3 L/min (work rate of 173 W) at 5050m high altitude for breathing during exercise was taken for the simulation. Weibel's model for flows in lung airways was used to obtain the corresponding flow rates and the inlet velocities at third generation for sea level and high altitude cases. The pressure was set to be zero at all outlets and no-slip boundary condition was imposed on all walls of the airway models [12-13]. Taking U.S. Standard Atmosphere Air Properties Data into consideration, the density and dynamic viscosity of air are $1.225 kg/m^3$ and $1.789\times10^{-5} kg/(ms)$ at sea level and about $0.7364 kg/m^3$ and $1.628\times10^{-5} kg/(ms)$ at 5050 high altitude.

2.4 Mesh Generation

After importing the 3D airway model in ANSYS Fluent 16.2 software, unstructured tetrahedral meshes with inflation layers were generated. Mesh independence study [8, 14-15] on the flow solution was performed by comparing the average velocity of five points on central path line p1 (Fig. 1) using grids consisting of 67,988 (N1), 210,986 (N2), 364,915 (N3), and 785,328 (N4). The steady simulation was implemented at each set of grids with inlet velocity 8m/s at 3rd generation. The increase grid of size from 364,915 to 785,328 alter the average velocity with relative error 0.0062(Table 2). Considering the available memory and computational time, a mesh with 364,915 grid size was adopted for the simulations.

Table 2. Results of mesh independency study

Number of elements	Mesh increment ratio(N_{i+1}/N_i)	Average velocity	Relative error
N_1 =67958	-	7.581692	-
N_2 =210986	3.10	7.868886	0.037880
N_3 =364915	1.73	8.061624	0.0244937
N_4 =785328	2.15	8.111704	0.006212

2.5 Numerical Method

The finite-volume based CFD software ANSYS Fluent 16.2 was used for the simulations of airflow in the constructed airway model. The governing equations were solved using a transient pressure based solver. The SIMPLE algorithm was applied in CFD solver for the pressure-velocity coupling. The second order discretization scheme was used for the pressure term and the second order upwind discretization scheme applied for momentum terms.

Considering the flow in pipes, the calculation of Reynolds number gives 2958, 1841, 1183, and 740 at sea level and 2878, 1790, 1151, and 719 at high altitude for third to sixth generations of the airway model. This shows the presence of laminar and transitional flow regimes in the respiratory airways during exercises. The unsteady state SST k-ω flow solver model with Low-Re corrections was used for this study. The SST model is one of the Reynolds-averaged Navier-Stokes (RANS) turbulence models which is more accurate and reliable for a wider class of flows as discussed by Elcner et al. [16]. A residual of less than was used as the convergence criteria. The duration of the whole breathing cycle during exercise is 1s, with inspiration and expiration lasting 0.5s each [17]. The flow time of 0.4s and time step size 0.0001s were used in the simulations.

3. Results and Discussion

The airflow characteristics, velocity, pressure, and wall shear stress were obtained from the CFD simulation results for breathing during exercise at sea level and high altitude. The results and comparison are presented in subsequent sections.

3.1 Velocity distribution

The velocity contours at the mid-plane (z = 0) for inspiratory airflow in the bifurcation model during exercise at sea level and at high altitude are presented in Fig. 2. It is observed that the values of the airflow velocity in the airway model are higher at high altitude than at sea level. From the simulations, the maximum velocity reached at sea level is 8.8508 m/s and at high altitude is 13.0488 m/s. The flow patterns for the two breathing conditions are presented using velocity stream lines in Fig. 3. The flow streamlines are highly turned to the wall at the bifurcations for the two breathing conditions. Figure 4 depicts the axial velocity contours on the cross-sections 1-4 at the middle of straight circular tube of the four generations (Fig. 1) for the two breathing conditions. It is observed that the magnitude of velocity is higher near to the anterior wall of the airway model. For further demonstration and comparison of inspiratory airflow for the two breathing conditions, the simulated velocity values were taken at 17 points on diameter of the cross section 2 of the left fourth generation from anterior to posterior direction and at 32 points on the central path line p2. The data are illustrated in Figs. 5 and 6. The distance is taken from anterior to posterior on the diameters of the cross section 2. The vertical distance is measured from the central point of the inlet of third generation to the point of consideration on the path line. Figure 5 shows that the values of simulated velocities are higher near the anterior wall on the cross-section for the two breathing conditions. The range of flow velocity values in the model is higher at high altitude than at sea level. The velocity values decrease relatively at the bifurcations as observed from Fig. 6. In general, there is no significant difference between the airflow structures for the two breathing conditions considered in the study even though there is a variation in magnitude of velocity as observed in Fig. 2-6.

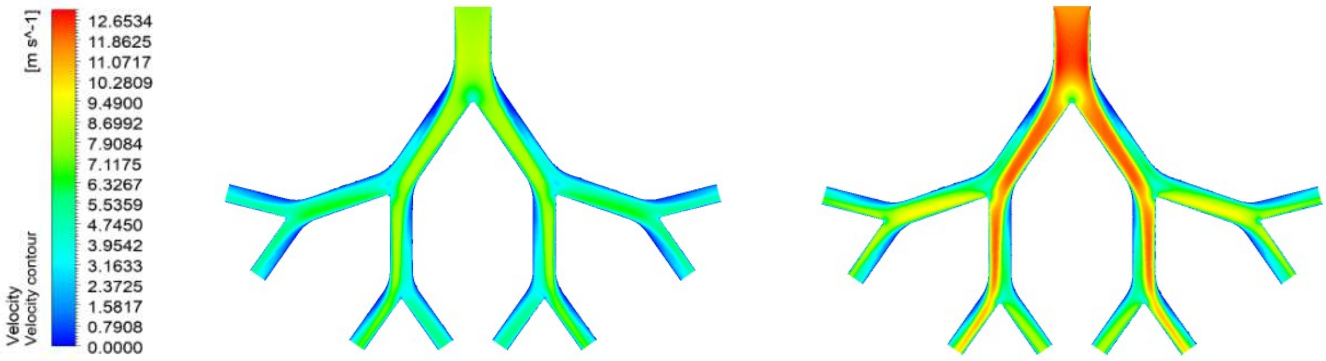

(a) (b)

Fig. 2. Inspiratory airflow velocity contour on mid-plane of the airway model during exercise at (a) sea level (b) high altitude

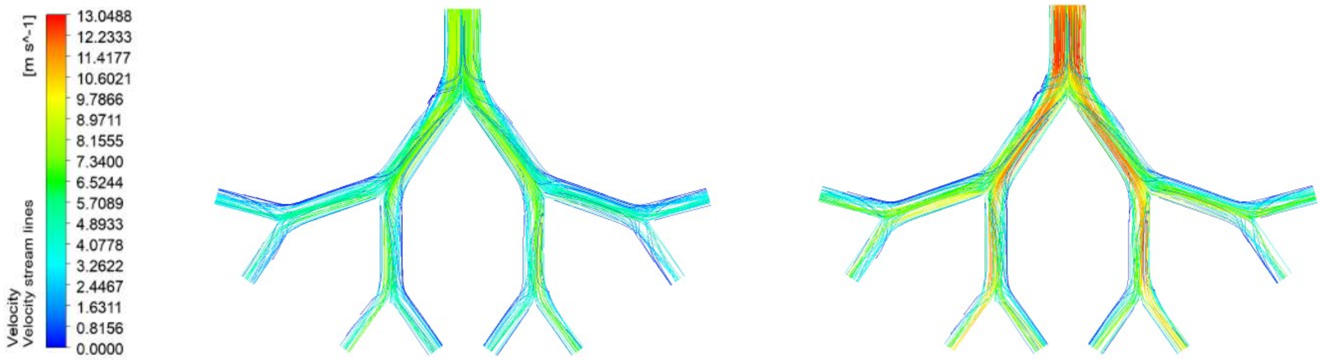

(a) (b)

Fig. 3. Inspiratory airflow velocity stream lines on the airway model during exercise at (a) sea level (b) high altitude

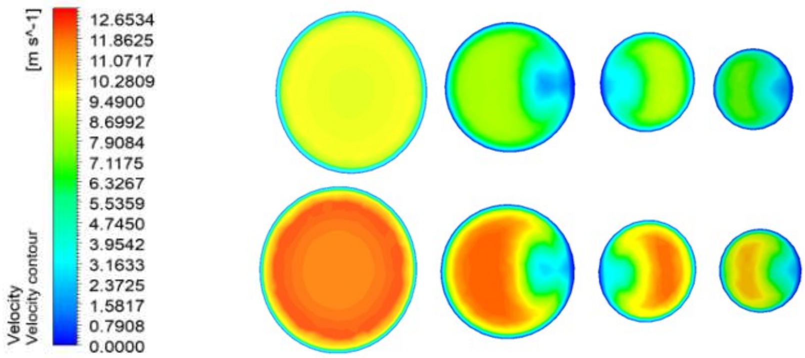

Fig. 4. The axial inspiratory airflow velocity contours at cross sections 1-4 during exercise (a) at sea level (b) at high altitude

3.2 Pressure distribution

The pressure contour on the mid-plane and wall of the airway model during exercise at sea level and at high altitude is shown in Figs. (7) and (8), respectively. The Figures show that the pressure is higher in the vicinity of the bifurcations and at the carinal edges in particular compared to the tubular zone in each branch of the airway for both breathing conditions. The maximum pressure attained in the flow is 38.1480 Pa at sea level and 52.1862 Pa at high altitude. The range of pressure values is higher at high altitude than sea level. The lowest pressure values are observed near the end of the third generation. As velocity, simulated pressure values were taken at 17 points of on diameter of the cross-section 2 from anterior to posterior direction and at 49 points on the central path line p2. The data are illustrated in Figs. 9 and 10. The shapes of the curves are similar in two breathing conditions, but the magnitude is different between the two curves.

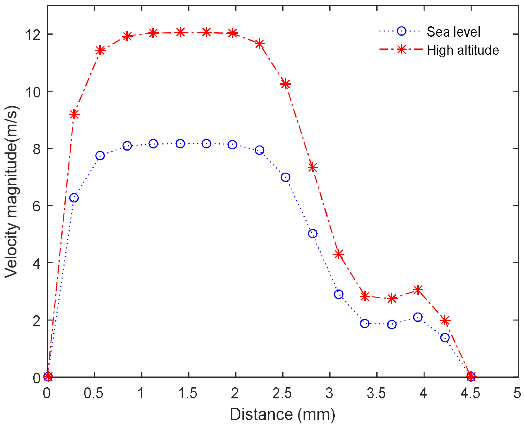

Fig. 5. velocity distribution on the diameter of the cross section 2

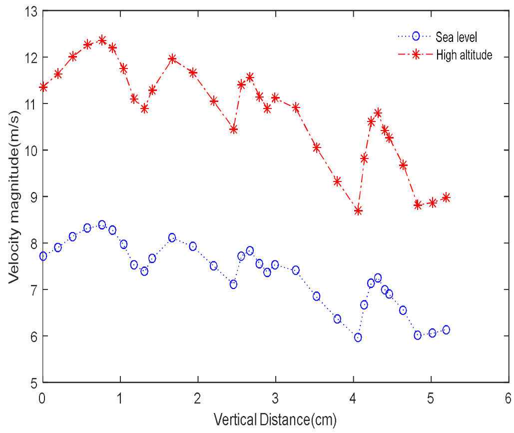

Fig. 6. velocity distributions on the path line p_2

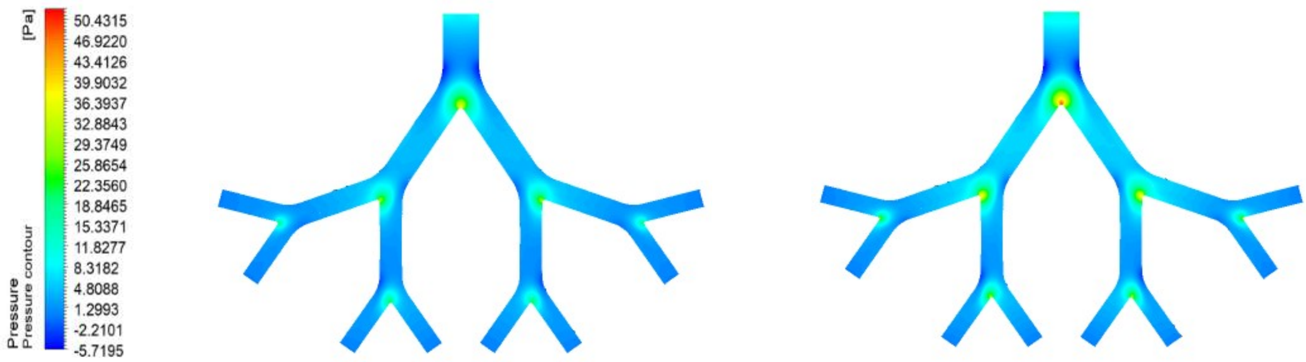

(a) (b)

Fig. 7. Inspiratory airflow pressure contour on mid-plane of the airway model during exercise at (a) sea level (b) high altitude

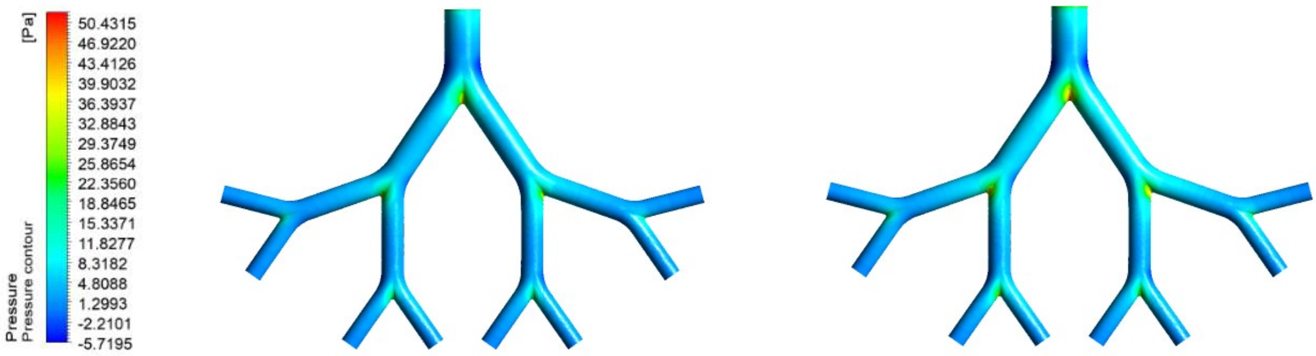

(a) (b)

Fig. 8. Inspiratory airflow pressure contour on wall of the airway model during exercise at (a) sea level (b) high altitude

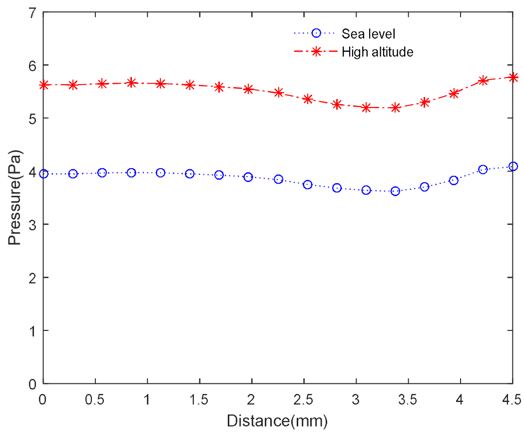

Fig. 9. Pressure distributions on diameter of the cross section 2

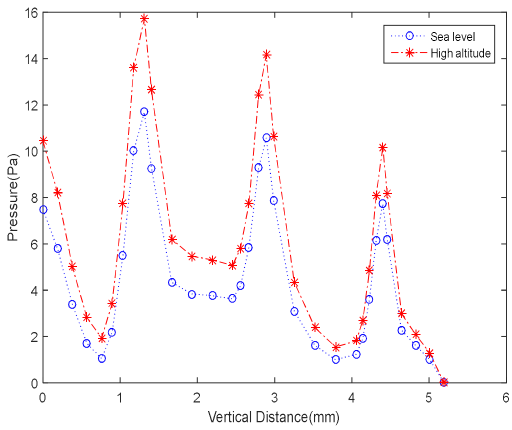

Fig. 10. Pressure distributions on central path line p2.

3.3 Wall shear stress distribution

The wall shear stresses of the simulated airflow in the airway model during exercise at sea level and at high altitude are illustrated in Fig. 11. In general, the values of wall shear stress are small on the air way model for the two breathing conditions. Like velocity and pressure, wall shear stress values are higher at high altitude than sea level. Wall shear stresses are highest at the inlet of the model.

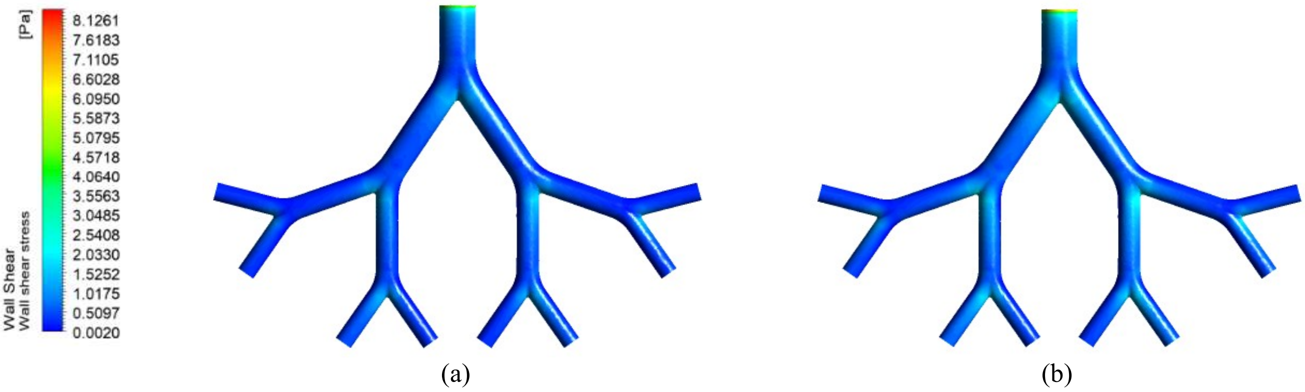

Fig. 11. Wall shear stress on the airway model for inspiratory airflow during exercise (a) at sea level (b) at high altitude

4. Conclusions

In this study, a numerical simulation of inspiratory airflow in human airway model during exercise at sea level and at high altitude was performed using the commercial software ANSYS Fluent. The governing equations of the unsteady airflow (Continuity and Navier-Stokes equations) in the airway model were solved with appropriate boundary conditions including the respiratory system responses to exercise at sea level and at high altitude. The quantitative results of this study showed that performing exercise at high altitude increases inspiratory airflow velocity, pressure, and wall shear stress more than at sea level in the airway model. The ranges of the airflow fields were also higher at high altitude than at sea level. It is observed in the simulation results that distributions of flow velocity, pressure, and wall shear stress in the airway model for the sea level and high altitude are generally similar in shape but different in magnitude.

Acknowledgment

We express our thanks to Institute of Computer Centre, IIT Roorkee for providing us with necessary software packages we used in this study including ANSYS Fluent 16.2 and MATLAB R2015a. We also thank the Department of Mechanical & Industrial Engineering, IIT Roorkee for providing us SOLIDWORKS 2013 software.

Conflict of Interest

The authors declare no conflict of interest.

References

[1] Cibella, F., Cuttitta, G., Kayser, B., Narici, M., Romano, S., Saibene, F., Respiratory mechanics during exhaustive submaximal exercise at high altitude in healthy humans, *Journal of Physiology* 494 (1996) 881-890.
[2] Aiken, M., Altitude Training for Everyone, 2013, https://www.runnersworld.com/race-training/altitude-training-for-everyone.
[3] Wehrlin, J.P., Hallén, J., Linear decrease in VO2max and performance with increasing altitude in endurance athletes, *European Journal of Applied Physiology* 96 (2005) 404-412.
[4] Sheel, A.W., MacNutt, M.J., Querido, J.S., The pulmonary system during exercise in hypoxia and the cold, *Experimental Physiology* 95 (2010) 422-430.
[5] Augusto, L.L.X., Lopes, G.C., Gonçalves, J.A.S., A CFD study of deposition of pharmaceutical aerosols under different respiratory conditions, *Brazilian Journal of Chemical Engineering* 33 (2016) 549-558.
[6] Weibel, E.R., *Morphometry of the Human Lung*. Springer Verlag, New York, 1963.
[7] Deng, Q., Ou, C., Chen, J., Xiang, Y., Particle deposition in tracheobronchial airways of an infant, child and adult, *Science of the Total Environment* 612 (2017) 339-346.
[8] Srivastav, V.K., Paul, A.R., Jain, A., Computational fluid dynamics study of airflow and particle transport in third to sixth generation human respiratory tract, *International Journal of Emerging Multidisciplinary Fluid Sciences* 3(4) (2012) 227-234.
[9] Hegedűs, C.J., Balásházy, Z.Y.I., Farkas, Á., Detailed mathematical description of the geometry of airway bifurcations, *Respiratory Physiology & Neurobiology* 141 (2004) 99-114.
[10] Ou, C., Deng, Q., Liu, W., Numerical simulation of particle deposition in obstructive human airways, *Journal of Central South University* 19 (2012) 609-614.

[11] Ou, C., Li, Y., Wei, J., Yen, H.L., Deng, Q., Numerical modeling of particle deposition in ferret airways: A comparison with humans, *Aerosol Science and Technology* 51(4) (2017) 477-487.
[12] Liu, Y., So, R.M.C., Zhang, C.H., Modeling the bifurcating flow in a human lung airway. *Journal of Biomechanics* 35 (2002) 477-485.
[13] Gemci, T., Ponyavin, V., Chen, Y., Chen, H., Collins, R., Computational model of airflow in upper 17 generations of human respiratory tract, *Journal of Biomechanics* 41 (2008) 2047-2054.
[14] Rahimi-Gorji, M., Gorji, T.B., Gorji-Bandpy, M., Details of regional particle deposition and airflow structures in a realistic model of human tracheobronchial airways: two-phase flow simulation. *Computers in Biology and Medicine* 74 (2017) 1-17.
[15] Qi, S., Zhang, B., Teng, Y., Li, J., Yue, Y., Kang, Y., Qian, W., Transient dynamics simulation of airflow in a CT-scanned human airway tree: more or fewer terminal bronchi? *Computational and Mathematical Methods in Medicine* 2017(3) (2017) 1-14.
[16] Elcner, J., Lizal, F., Jedelsky, J., Jicha, M., Chovancova, M., Numerical investigation of inspiratory airflow in a realistic model of the human tracheobronchial airways and a comparison with experimental results, *Biomechanics and Modeling in Mechanobiology* 15(2) (2016) 447–469.
[17] Johnson, T., *Biomechanics and Exercise Physiology: Quantitative Modeling*, Second edition, CRC press, New York, 2007.